

RESEARCH ARTICLE

[View Article Online](#)
[View Journal](#) | [View Issue](#)



Cite this: *Inorg. Chem. Front.*, 2024, 11, 6919

Chemical modulation of $A^I RE^{III} C^{IV} Q_4^{VI}$ family compounds for band gap and optical anisotropy enhancement†

Hongshan Wang,^{a,b} Xueting Pan,^a Shilie Pan^{id, *a,b} and Junjie Li^{id, *a,b}

Rare-earth (RE) compounds show wide applications in advanced photoelectric functional materials. Herein, by introducing $[AgS_3]$ trihedral and $[NaQ_6]$ ($Q = S, Se$) octahedral units into the $A^I RE^{III} C^{IV} Q_4^{VI}$ family for the first time, four new RE-based chalcogenides $A^I RE^{III} SiQ_4^{VI}$ ($A^I = Ag, Na; RE^{III} = La, Y; Q^{VI} = S, Se$) were designed and successfully synthesized. With the increase of atomic radius from Ag, Li, Na, K, to Rb and Cs, the compounds show evident structural transitions from $Ama2$ ($LiLaSiS_4$), $P2_1/c$ ($AgLaSi_4$, $NaLaSiS_4$), and $P2_1$ ($KLaSiS_4$) to $Pnma$ ($RbLaSiS_4$, $CsLaSiS_4$), highlighting that chemical modulations including atomic radius, coordination and bond length co-affected the structure transition. The title compounds exhibit wide band gaps (3.33 and 3.18 eV for $AgLaSiS_4$ and $AgYSiS_4$; 3.83 and 3.02 eV (HSE06) for $NaLaSiS_4$ and $NaLaSiSe_4$, respectively) that are higher than the Ag- and RE-based chalcogenides, as well as strong optical anisotropies ($\Delta n_{cal} = 0.114-0.160$ at 1064 nm). The theoretical calculations confirm the charge transfer enhanced band gap mechanism in the compounds and demonstrate that the layer distance influenced birefringence. The results enrich the chemical and structural diversity of RE compounds in the $A^I RE^{III} C^{IV} Q_4^{VI}$ family and give new insights into the design of new RE-based compounds with wide band gaps and large birefringence.

Received 10th July 2024,
Accepted 14th August 2024

DOI: 10.1039/d4qi01738b

rsc.li/frontiers-inorganic

Introduction

The development of new functional materials is highly dependent on the discovery of new compounds with distinctive crystal structures and physicochemical properties.¹⁻⁶ Chalcogenides show abundant structural and chemical diversities, wide infrared (IR) transmission ranges, and adjustable optical properties, which are widely used in the fields of photo-detection, nonlinear optical (NLO) applications, light polarization, and photo-catalysis, making them an essential natural treasure trove for the exploration of advanced photoelectric functional materials.⁷⁻¹¹ Over the past few decades, by combining different fundamental building block groups,¹²⁻¹⁴ a large number of metal chalcogenides have been developed, such as $Cs_3In(In_4Se_7)(P_2Se_6)$,¹⁵ $Sn_7Br_{10}S_2$,¹⁶ and $SrB^{II}GeS_4$ ($B^{II} =$

Zn, Hg ^{17,18} with strong NLO response as well as $Rb_3NaSn_3Se_8$ ¹⁹ and $Na_2HgSn_2Se_6$ ²⁰ with large optical anisotropy.

To increase the functional diversity, introducing rare-earth (RE) elements with a unique f-electron configuration, strong positive charge, and multiple coordination environments into the structural design of chalcogenides has been demonstrated as a feasible strategy.²¹⁻²⁴ More recently, Yu and coworkers reported the synthesis of the first stable La^{2+} -based chalcogenide $LaMg_6Ga_6S_{16}$, in which the La^{2+} is six-coordinated with S atoms.²⁵ The compound exhibits a wide green emission band at 500 nm, as well as a strong NLO response ($\sim 1 \times AgGaS_2$), a wide band gap ($E_g = 3.0$ eV) and a high laser-induced damage threshold ($\sim 5 \times AgGaS_2$).²⁵ Remarkably, the relatively large size of the standard RE^{3+} ion radius can accommodate higher coordination numbers (up to ~ 12).²³ The abundant coordination modes lead to multiple crystal structures in RE-contained chalcogenides, such as in $RE_3^{III}GaS_6$ ($RE^{III} = Y, Dy, Ho$, and Er),²⁶ $Ba_2RE^{III}M^{III}Se_5$ ($RE^{III} = Y, Ce, Nd, Sm, Gd, Dy$, and Er ; $M^{III} = Ga, In$),²⁷ $La_3LiM^{IV}S_7$ ($M^{IV} = Ge, Sn$),²⁸ and $A^I RE^{III} C^{IV} Q_4^{VI}$ ($A^I = Li, K, Rb, Cs; RE^{III} = Y, La-Nd, Sm-Yb; C^{IV} = Si, Ge; Q^{VI} = S, Se$).^{1,29-31}

In the $A^I RE^{III} C^{IV} Q_4^{VI}$ family, many attempts have been made and more than 50 compounds have been synthesized. Among them, the A^I -site atom is usually occupied by Li, K, Rb or Cs,

^aResearch Center for Crystal Materials; State Key Laboratory of Functional Materials and Devices for Special Environmental Conditions; Xinjiang Key Laboratory of Functional Crystal Materials; Xinjiang Technical Institute of Physics and Chemistry, CAS, 40-1 South Beijing Road, Urumqi 830011, China. E-mail: slpan@ms.xjb.ac.cn, lijunjie@ms.xjb.ac.cn

^bCenter of Materials Science and Optoelectronics Engineering, University of Chinese Academy of Sciences, Beijing 100049, China

† Electronic supplementary information (ESI) available. CCDC 2368926–2368929. For ESI and crystallographic data in CIF or other electronic format see DOI: <https://doi.org/10.1039/d4qi01738b>

while the syntheses of Na-/Ag-containing compounds have still not been achieved, similar to the case in the $A^I B_4 O_6 F$ ($A^I = NH_4, Na, Rb, Cs$) family (where the synthesis of $Li/KB_4 O_6 F$ is yet to be achieved) famous for their excellent NLO properties in the UV regions.^{32–34} In this work, Na- and Ag-containing systems were investigated, and four new RE chalcogenides $A^I RE^{III} SiQ_4^{VI}$ ($A^I = Ag, Na; RE^{III} = La, Y; Q^{VI} = S, Se$) have been synthesized by the high temperature solution method in sealed quartz tubes. Based on structural investigations in the Inorganic Crystal Structure Database (ICSD version 5.0.0 (build 20230418-1517)), and to the best of our knowledge, they are the first series of Na- and Ag-containing compounds in the $A^I RE^{III} C^IV Q_4^{VI}$ family. The compounds crystallize in the centrosymmetric (CS) $P2_1/c$ space group that is different from the commonly appearing non-centrosymmetric (NCS) $P2_1, Ama2$ and CS $Pnma$ space groups in the Li-, K-, Rb-, Cs-containing compounds in this family. The compounds show wide band gaps (3.18 and 3.33 eV for $AgYSiS_4$ and $AgLaSiS_4$; 3.83 and 3.02 eV (HSE06) for $NaLaSiS_4$ and $NaLaSiSe_4$, respectively), strong optical anisotropy and large birefringence from 0.114@1064 nm for $AgLaSiS_4$ to 0.160@1064 nm for $NaLaSiSe_4$. In addition, theoretical calculations reveal that the wide band gap in the title compounds is mainly attributed to the charge transfer enhanced band gap mechanism between $[REQ_8]$ and $[SiQ_4]$ groups.

Experimental section

Raw materials

Raw materials utilized for the experimental syntheses, such as Na (99.9%), Ag (99.9%), La (99.99%), Y (99.99%), Si (99.9%), S (99.9%) and Se (99.9%), were purchased from the Shanghai Aladdin Biochemistry Technology Co., Ltd. To prevent oxidation and deliquescence of the materials, all starting materials were preserved and weighed in an Ar gas-filled glove box.

Chemical syntheses

The single crystals of $AgLaSiS_4$, $AgYSiS_4$, $NaLaSiS_4$, and $NaLaSiSe_4$ for structural determinations were fabricated by the high temperature solution method as follows: (1) Ag/Na, La/Y, Si, and S/Se materials with a molar ratio of 1:1:1:4 were mixed initially and loaded into quartz tubes with an inner diameter of 10 mm; (2) the quartz tubes were sealed with a hydrogen–oxygen flame under a high vacuum of 10^{-3} Pa; (3) the sealed samples were put into a Muffle furnace with the following programmed temperature: heated at $7\text{ }^{\circ}\text{C h}^{-1}$ from room temperature to $900\text{ }^{\circ}\text{C}$, maintained at this temperature for 75 h, then slowly cooled to room temperature at $6\text{ }^{\circ}\text{C h}^{-1}$. After that, the light yellow single crystals of $AgLaSiS_4$, $AgYSiS_4$, and $NaLaSiS_4$, and the yellow single crystals of $NaLaSiSe_4$ were harvested.

The polycrystalline powder samples of $AgLaSiS_4$ and $AgYSiS_4$ were synthesized by a similar procedure with the chemical stoichiometric ratios of $Ag:La/Y:Si:S = 1:1:1:4$,

and the holding time at the temperatures (900 $^{\circ}\text{C}$ for $AgLaSiS_4$ and 930 $^{\circ}\text{C}$ for $AgYSiS_4$) was set to 100 h. It is worth noting that the syntheses of the polycrystalline $NaLaSiQ_4^{VI}$ ($Q^{VI} = S, Se$) pure phase powder samples were also tried, but they failed.

Structure determination

The single-crystal diffraction data of the title compounds were collected on a Bruker APEX II charge-coupled device (CCD) diffractometer equipped with monochromatic Mo K_{α} radiation ($\lambda = 0.71073\text{ \AA}$) at room temperature.^{35,36} The absorption correction was performed by the multi-scan method. The crystal structures were determined directly and refined through a full matrix with least squares fit on F^2 by the structure resolution program package SHELXTL on Olex2 v1.2.^{37,38} The PLATON program was used to detect possible missing symmetry elements, and no higher symmetries were found in the crystal structures.

Powder X-ray diffraction (PXRD)

To check the purity of the obtained polycrystalline powder samples, the PXRD patterns of $AgLaSiS_4$ and $AgYSiS_4$ were collected on an automated Bruker D2 bit-phase diffractometer with Cu target K_{α} radiation ($\lambda = 1.5418\text{ \AA}$). The diffraction data were recorded from 10 to 70° (2θ ranges) with a scan step width of 0.02° and a fixed counting time of 1 s per step at room temperature.

Energy-dispersive X-ray spectroscopy (EDS) analyses

The EDS spectra and mappings of the title compounds were conducted on a field emission scanning electron microscope (FE-SEM, JEOL JSM-7610F Plus, Japan) at 298 K with an energy-dispersive X-ray spectrometer (Oxford, X-Max 50) at 5 kV.

UV-vis-NIR diffuse reflectance spectroscopy

Diffuse-reflectance spectra of the polycrystalline $AgRE^{III} SiS_4$ ($RE^{III} = La, Y$) powder samples were obtained on a Shimadzu SolidSpec-3700 DUV spectrophotometer over the wavelength range of 200–2600 nm at room temperature,³⁹ and $BaSO_4$ served as the reference. The experimental optical band gaps (E_g) were determined by converting the diffuse reflection data to absorption data through the Kubelka–Munk function, $F(R) = K/S = (1 - R)^2/2R$, where R denotes the reflection coefficient, K is the absorption value, and S is the scattering coefficient.

Raman spectra

The Raman spectra of the four compounds were measured on a LABRAM HR Evolution spectrometer (Japan) fitted with a CCD detector operating at 532 nm radiation and were acquired from 4000 to 100 cm^{-1} (2.5–100 μm).

Theoretical calculations

The band structures, partial and total density of states (P/TDOS), and birefringence of the title compounds were computed by the plane wave pseudopotential method in CASTEP.^{40,41} The electronic structures of the compounds were

analyzed by density functional theory (DFT) with the Perdew–Burke–Ernzerhof (PBE) exchange–correlation function in the generalized gradient approximation (GGA).⁴² Meanwhile, the band gaps of the title compounds were investigated by the PWmat code utilizing the Heyd–Scuseria–Ernzerhof (HSE06) hybrid functional, with a plane wave cutoff of 50 eV.⁴³ The interactions between the ionic core and electrons were described by norm-conserving pseudopotentials (NCP). The valence electron configurations of Ag 4d¹⁰5s¹, Na 2p⁶3s¹, La 5d¹6s², Y 5s²4d¹, Si 3s²3p², S 3s²3p⁴ and Se 4s²4p⁴ were considered during the calculations. A cutoff energy of 800 eV was utilized. The Monkhorst–Pack *k*-point in the Brillouin zone (BZ) was set to 0.035 Å^{−1}. The refractive indices were theoretically derived from the real part of the dielectric function using the Kramers–Kronig transform.⁴⁴

Results and discussion

Crystal structures

Transparent AgLaSiS₄, AgYSiS₄, NaLaSiS₄, and NaLaSiSe₄ single crystals for structure determination were picked under an optical microscope. The results of single-crystal XRD show that the four compounds crystallize in the same space group (Table S1†) and show similar structural features (Fig. 1 and S1–S3†). Therefore, AgLaSiS₄ is utilized as an example to illustrate their crystal structures herein. AgLaSiS₄ crystallizes in the monoclinic *P*2₁/c (no. 14) space group with cell parameters *a* = 8.9451(8) Å, *b* = 10.5565(9) Å, *c* = 6.9470(6) Å, *Z* = 4. In its asymmetric unit, there is one crystallographically independent Ag, one La, one Si, and four S atoms, and the atoms are all located at Wyckoff 4e positions. The Ag atoms are coordinated with three S atoms to build the [AgS₃] triangle planar units with the Ag–S bond lengths of 2.490–2.615 Å (Fig. 1a). The Si atoms are bonded with four S atoms to form [SiS₄] tetrahedra with Si–S bond lengths of 2.086–2.140 Å (Fig. 1b). The La atoms are connected with eight S atoms to construct the [LaS₈] polyhedral units with La–S bond lengths of 2.916–3.136 Å (Fig. 1c). The

resulting [SiS₄] and [LaS₈] units are edge-shared into a [LaSiS₁₀] dimer (Fig. 1d), which further extends by vertex-sharing into a serpentine [LaSiS₁₀]_∞ layer (Fig. 1g). Furthermore, the formed [AgS₃] unit pseudo-layers are located between the serpentine [LaSiS₁₀]_∞ layers, constructing the final three-dimensional (3D) crystal structure of AgLaSiS₄ (Fig. 1e and f). It is worth mentioning that NaLaSiQ₄ (Q = S, Se) shows a similar crystal structure to AgRE^{III}SiS₄ (RE^{III} = La, Y), but the Na atoms are 6-coordinated in the former that is different to the 3-coordinated Ag atoms in the latter, giving rise to an enhanced layer spacing in NaLaSiQ₄ (Q^{VI} = S, Se).

The detailed crystal data, atomic coordinate equivalent isotropic displacement parameters, bond valence sum (BVS), selected bond lengths, and bond angle data of the title compounds are provided in Tables S1–S17,† respectively. The calculated bond valence sums (BVSs) and global instability indexes (GIIs) (Tables S2–S5†) verify the reasonability of the crystal structures. To check the chemical compositions, EDS spectra and element mappings of the four compounds were carried out. The results confirm the presence of elements Ag/Na, La/Y, Si, and S/Se in A^IRE^{III}SiQ₄ (A^I = Ag, Na; RE^{III} = La, Y; Q^{VI} = S, Se) and the element ratios (Ag:La:Si:S = 1.10:1.03:1.03:4.00 in AgLaSiS₄, Ag:Y:Si:S = 1.06:1.09:1.11:4.00 in AgYSiS₄, Na:La:Si:S = 1.16:1.02:0.99:4.00 in NaLaSiS₄, and Na:La:Si:Se = 0.97:0.98:0.96:4.00 in NaLaSiSe₄) show good agreement with the values according to their chemical formulae (Fig. S4†). To further confirm the chemical bonding, the Raman spectra of the compounds were characterized. As shown in Fig. S5,† the peaks at 62.25–266.56 cm^{−1} in AgLaSiS₄ (59.98–259.03 cm^{−1} in AgYSiS₄) can be assigned to the vibrations of Ag–S and La–S (Ag–S and Y–S) bonds;^{11,25,45,46} while the peaks between 73.81–287.15 cm^{−1} in NaLaSiS₄ (59.98–183.98 cm^{−1} in NaLaSiSe₄) can be attributed to the vibrations of Na–S and La–S (Na–Se and La–Se) bonds;^{11,25,47} the peak at 397.67/408.01/399.07 cm^{−1} in AgLaSiS₄/AgYSiS₄/NaLaSiS₄ (228.47 and 250.37 cm^{−1} in NaLaSiSe₄) is related to the characteristic vibrations of Si–S or Si–Se bonds.^{48–50}

Based on the structural investigations in the ICSD (version 5.0.0, build 20230418-1517), the A-site is usually occupied by K, Rb, or Cs atoms in the A^IRE^{III}C^{IV}Q₄^{VI} family, and the title compounds are the first Na- and Ag-containing compounds in the family (Fig. 2a). Moreover, it can be seen that the A^IRE^{III}C^{IV}Q₄^{VI} family compounds (61 cases) are generally crystallized in the *P*2₁ (no. 4) and *P*2₁2₁2₁ (no. 19) space groups, and the number of compounds that crystallize in the *P*2₁/m (no. 11), *P*2₁/c (no. 14), *Pnma* (no. 62), and *Ama*2 (no. 40) space groups are quite rare (Table S18† and Fig. 2b).

To illustrate the A-site atom affected crystal structures in the A^IRE^{III}C^{IV}Q₄^{VI} family, a detailed structural analysis on A^ILaSiS₄ (A^I = Li, Ag, Na, K, Rb, Cs) was carried out, as shown in Fig. 3. It can be seen that: (i) with the increase of atomic radius from Li, Na, K, to Rb and Cs, the compounds show evident structural transitions from *Ama*2 (LiLaSiS₄)³¹ *P*2₁/c (NaLaSiS₄), and *P*2₁ (KLaSiS₄)³⁰ to *Pnma* (RbLaSiS₄, CsLaSiS₄)^{51,52} (Fig. 3a–d). Meanwhile, A^ILaSiS₄ (A^I = Ag, Na, K,

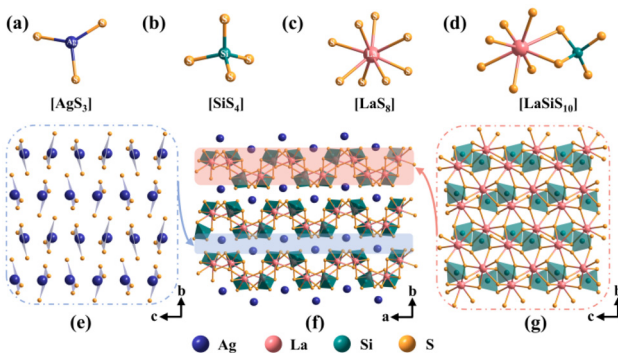


Fig. 1 Crystal structure of AgLaSiS₄. (a–c) The coordination environments of Ag, Si, and La atoms in the compound; (d) the formed [LaSiS₁₀] dimer; (e) the formed [AgS₃] pseudo-layers in AgLaSiS₄; (f) the 3D crystal structure of AgLaSiS₄ viewed along the *c* direction; (g) the formed 2D [LaSiS₁₀]_∞ layers viewed along the *a* direction.

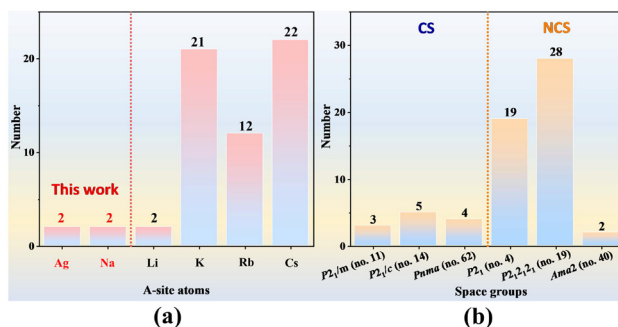


Fig. 2 Statistical analyses showing the different A-site atoms (a) and space groups (b) in the $A^1RE^{III}C^{IV}Q^{VI}$ ($A^1 = \text{Ag, Li-Cs; RE}^{III} = \text{Y, La-Nd, Sm-Yb; } C^{IV} = \text{Si, Ge; } Q^{VI} = \text{S, Se}$) family compounds.

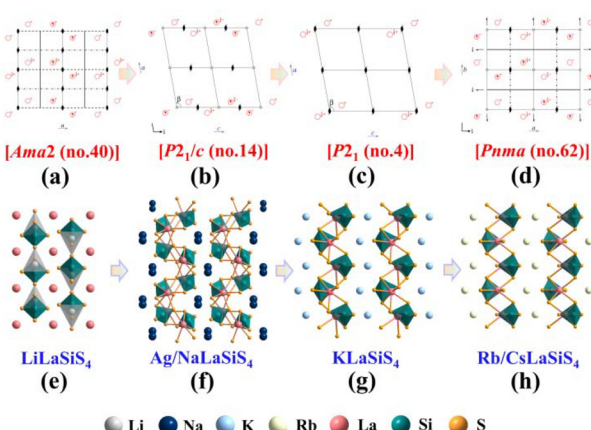


Fig. 3 Structural fluctuations in $A^1\text{LaSiS}_4$ ($A^1 = \text{Li, Ag, Na, K, Rb, Cs}$): (a-d) symmetry changes from $\text{Ama}2$ (LiLaSiS_4), $\text{P}2_1/c$ ($\text{AgLaSiS}_4/\text{NaLaSiS}_4$), and $\text{P}2_1$ (KLaSiS_4) to Pnma (RbLaSiS_4 and CsLaSiS_4); (e-h) the crystal structures of LiLaSiS_4 (e), Ag/NaLaSiS_4 (f), KLaSiS_4 (g), and Rb/CsLaSiS_4 (h).

Rb, Cs) shows a similar framework structure composed of $[\text{LaS}_8]$ and $[\text{SiS}_4]$, different from the $[\text{LaSiS}_{11}]_\infty$ framework built by $[\text{LaS}_8]$ and $[\text{SiS}_4]$ in LiLaSiS_4 (Fig. 3e-h and S6 \dagger); (ii) since the Ag atom is 3-coordinated with S atoms, the formed $[\text{AgS}_3]$ units in AgLaSiS_4 are isolated from others to form a pseudo-layer structure, different to the formed Na/K/Rb/Cs-S layer structure built by $[\text{NaS}_6]$ octahedra or $[\text{K/Rb/CsS}_8]$ polyhedra in $A^1\text{LaSiS}_4$ ($A^1 = \text{Na, K, Rb, Cs}$), confirming that the coordination mode affected crystal structures (Fig. S7 \dagger); (iii) compared to the shorter Ag-S bond length (2.4897–2.6149 Å) in AgLaSiS_4 , the longer Na-S bond length (2.780–3.267 Å) results in a larger layer spacing of 9.314 Å in NaLaSiS_4 (8.945 Å for AgLaSiS_4). RbLaSiS_4 and CsLaSiS_4 exhibit a similar phenomenon, and the layer spacing is increased from 8.642 Å in RbLaSiS_4 to 8.932 Å in CsLaSiS_4 (Fig. S8 \dagger). The results highlight that atomic radius, coordination number, and bond length (related to A-site atoms) co-affected the crystal structure in the $A^1\text{RE}^{III}C^{IV}Q^{VI}$ family.

Optical properties

To investigate the optical properties of the compounds, the pure-phase polycrystalline powder samples of AgLaSiS_4 and AgYSiS_4 were successfully prepared and characterized. The experimental XRD patterns of the two compounds match well with the theoretical results from their CIF files (Fig. 4a and b), confirming the single crystal structures and high purity for the obtained polycrystalline powder samples. To evaluate the experimental band gaps, UV-vis-NIR diffuse reflectance spectra were measured on the pure phase powder samples. Based on the Kubelka-Munk function, the experimental band gaps of AgLaSiS_4 and AgYSiS_4 were determined to be ~ 3.33 eV and ~ 3.18 eV, respectively (Fig. 4c and d), which are comparable to the results in recently developed wide band gap chalcogenides like $\text{Zn}_2\text{HgP}_2\text{S}_8$ (3.37 eV),⁵³ $\text{LiMGa}_8\text{S}_{14}$ ($\text{M} = \text{Rb/Ba, Cs/Ba}$) (3.24–3.32 eV),⁵⁴ $\text{Ca}_2\text{La}(\text{BS}_3)(\text{SiS}_4)$ (3.38 eV),⁵⁵ $[\text{Ba}_4(\text{S}_2)][\text{ZnGa}_4\text{S}_{10}]$ (3.39 eV)⁵⁶ and $\text{Na}_2\text{Ba}[\text{Na}_2\text{Sn}_2\text{S}_7]$ (3.42 eV),⁵⁷ but smaller than the RE-based oxychalcogenide $\text{Nd}_3[\text{Ga}_3\text{O}_3\text{S}_3][\text{Ge}_2\text{O}_7]$ (4.35 eV).⁵⁸ Interestingly, Ag-based chalcogenides like AgGaS_2 (2.64 eV),⁵⁹ $\text{Ag}_2\text{In}_2\text{SiS}_6$ (2.41 eV),⁶⁰ $\text{Ag}_2\text{In}_2\text{GeS}_6$ (2.3 eV),⁶¹ $\text{Li/NaAgIn}_2\text{GeS}_6$ (2.47/2.40 eV),⁶¹ and AgHgPS_4 (2.63 eV),⁶² as well as RE-based chalcogenides, such as $\text{RE}_2\text{B}^{\text{II}}_3\text{Sn}_3\text{S}_{12}$ ($\text{RE}^{III} = \text{La, Sm, Gd; B} = \text{Ca, Sr}$) (1.51–1.71 eV),⁶³ $\text{La}_6\text{B}^{\text{II}}_3\text{GeS}_{14}$ ($\text{B}^{III} = \text{Ga, In}$) (2.54–2.61 eV),⁶⁴ and $\text{EuB}^{\text{II}}\text{C}^{IV}\text{Q}^{VI}$ ($\text{B}^{\text{II}} = \text{Cd, Hg; C}^{IV} = \text{Ge, Sn; Q}^{VI} = \text{S, Se}$) (1.97–2.50 eV),^{65,66} usually exhibit small band gaps that limit their applications, while both Ag and RE containing compounds AgLaSiS_4 (3.33 eV) and AgYSiS_4 (3.18 eV) in this work display wide band gaps, breaking through the “3.0 eV wall” of energy band gap in the Ag and RE coexisting chalcogenides. To check the physical and chemical stability, $A^1\text{RE}^{III}\text{SiQ}^{VI}$ single crystals were picked and placed in water for 7 days. The optical images (Fig. S9 \dagger) confirm that the title compounds have a good chemi-

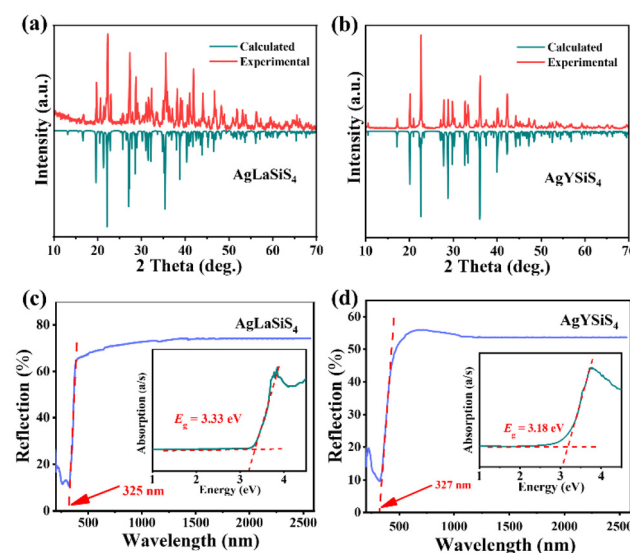


Fig. 4 The experimental and calculated XRD patterns of (a) AgLaSiS_4 , and (b) AgYSiS_4 ; the UV-vis-NIR diffuse reflectance spectra and experimental band gaps of (c) AgLaSiS_4 , and (d) AgYSiS_4 .

cal stability in water. Moreover, the polycrystalline $\text{AgRE}^{\text{III}}\text{Si}_4$ powder samples were exposed in the air for 6 months, and no changes have been observed in the XRD patterns before and after the exposure (Fig. S10†), indicating the compounds are air stable.

Theoretical calculations

To clarify the origin of optical band gaps of the title compounds, first-principles calculations were carried out. The calculated band structures indicate that $\text{A}^{\text{I}}\text{RE}^{\text{III}}\text{Si}_4^{\text{VI}}$ are indirect band gap compounds. The calculated GGA band gaps are 2.398 eV for AgLaSi_4 , 2.274 eV for AgYSi_4 , 2.873 eV for NaLaSi_4 , and 2.282 eV for NaLaSiSe_4 (Fig. 5a and S11a–c†). Due to the discontinuity of the exchange–correlation energy function, the GGA band gap is usually underestimated.^{67,68} Thus, the HSE06 functional was employed to guarantee the accuracy and consistency of the theoretical band gaps, and the resulted HSE06 band gaps are 3.56 eV for AgLaSi_4 , 3.34 eV for AgYSi_4 , 3.83 eV for NaLaSi_4 , and 3.02 eV for NaLaSiSe_4 , which are close to the experimental values of the selected AgLaSi_4 (3.33 eV) and AgYSi_4 (3.18 eV). The results of T/PDOS indicate that the valence band (VB) maximum is mainly occupied by Ag-d, La-d, S-p orbitals in AgLaSi_4 ; Ag-d, Y-d, S-p orbitals in AgYSi_4 ; La-d, S-p orbitals in NaLaSi_4 ; and La-d, Se-p orbitals in NaLaSiSe_4 , and the conduction band (CB) minimum is mainly occupied by La-d, Si-p, S-p orbitals in AgLaSi_4 ; Y-d, Si-p, S-p orbitals in AgYSi_4 ; La-d, Si-p, S-p orbitals in NaLaSi_4 ; and La-d, Si-p, Se-p orbitals in NaLaSiSe_4 (Fig. 5b and S11d–f†). It implies that the optical band gap is mainly determined by $[\text{AgS}_3]$ and $[\text{RES}_8]$ units in $\text{AgRE}^{\text{III}}\text{Si}_4$,

while $[\text{LaQ}_8]$ units determine the optical band gap in $\text{NaLaSi}_4^{\text{VI}}$. Further analyses on the T/PDOS structures confirm the charge transfer enhanced band gap mechanism in the compounds.¹ In contrast to La_2S_3 , where the La-d and S-p orbitals show a strong hybridisation in the –4.5–0 and 2.5–5 eV regions (indicated by the yellow region in Fig. S12b†), the d-p orbital hybridisation between La and S is significantly reduced in the same region, and an evident orbital hybridisation between the S-p orbitals and Si-p orbitals in the 2.5 to 5.0 eV regions (indicated by the blue and red regions in Fig. S12d†) is observed in AgLaSi_4 (taking AgLaSi_4 as an example herein), giving rise to the decreased covalency of La–S bonds by transferring notably charge from $[\text{LaS}_8]$ to $[\text{SiS}_4]$ units, thus resulting in a wide band gap in AgLaSi_4 . The other title compounds show similar charge transfer enhanced band gap mechanisms (Fig. S13 and 14†). In addition, compared to the hybridization regions (–0.43–0.71 eV) of Y-d, Si-p, and S-p orbitals near the bottom of the CB minimum in AgYSi_4 , the regions of La-d, Si-p, and S-p orbitals in AgLaSi_4 show a slight shift to –0.09–0.97 eV, resulting in a wider band gap in AgLaSi_4 (3.33 eV) than AgYSi_4 (3.18 eV), similar to the case in KLaGe_4 (3.34 eV)⁶⁹ and KYGe_4 (3.15 eV).¹

Moreover, due to the strong optical anisotropy in the crystal structures, the birefringence of the title compounds was calculated to be 0.114 (AgLaSi_4), 0.129 (AgYSi_4), 0.130 (NaLaSi_4), and 0.160 (NaLaSiSe_4) at 1064 nm (Fig. 5c and S11g–i†). Among them, NaLaSiSe_4 exhibits the largest known birefringence in the $\text{A}^{\text{I}}\text{RE}^{\text{IV}}\text{Q}_4^{\text{VI}}$ family compounds (Fig. 5d). Moreover, the birefringence discrepancy between AgLaSi_4 and NaLaSi_4 could be related to the fluctuation of layer spacing between $[\text{LaSi}_{10}]_{\infty}$ layers (8.945 Å for AgLaSi_4 , 9.314 Å for NaLaSi_4) induced by the fluctuation of Ag and Na atoms in the structures.⁷⁰ To confirm this point, a virtual AgLaSi_4 atom model (Fig. S15†) with a larger $[\text{LaSi}_{10}]_{\infty}$ layer spacing of 9.286 Å was built from NaLaSi_4 by atomic replacement, and its birefringence was computed to be $\Delta n = 0.123$ at 1064 nm, as shown in Fig. 5c. It means that along with the increase of layer spacing from 8.945 (experimental AgLaSi_4 model) to 9.286 Å (virtual AgLaSi_4 model), the birefringence in the built model is calculated to be 0.123 at 1064 nm, larger than the value (0.114 at 1064 nm) in the experimental model, indicating that the larger layer spacing is beneficial for producing larger birefringence.

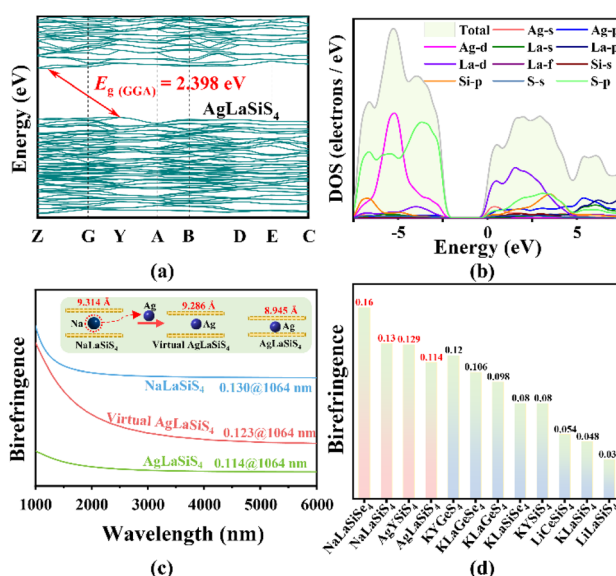


Fig. 5 The band structures (a) and the T/PDOS (b) of AgLaSi_4 ; (c) the calculated birefringence of AgLaSi_4 , virtual AgLaSi_4 , and NaLaSi_4 (inset diagrams show the fluctuation of layer distance in AgLaSi_4 , NaLaSi_4 and virtual AgLaSi_4 built from NaLaSi_4); (d) statistical birefringence (at 1064 nm) of title compounds and other compounds in the $\text{A}^{\text{I}}\text{RE}^{\text{IV}}\text{C}^{\text{IV}}\text{Q}_4^{\text{VI}}$ family.

Conclusions

In summary, four new RE compounds $\text{A}^{\text{I}}\text{RE}^{\text{III}}\text{Si}_4^{\text{VI}}$ ($\text{A}^{\text{I}} = \text{Ag, Na; RE}^{\text{III}} = \text{La, Y; Q}^{\text{VI}} = \text{S, Se}$) have been rationally designed, and synthesized by a high temperature solution method. To the best of our knowledge, the four compounds are the first series of Ag- or Na-containing compounds in the $\text{A}^{\text{I}}\text{RE}^{\text{III}}\text{C}^{\text{IV}}\text{Q}_4^{\text{VI}}$ family, enriching the chemical diversity of the family. The four compounds crystallize in the same $P2_1/c$ space group and are constructed with $[\text{AgS}_3]$, $[\text{RES}_8]$, and $[\text{SiS}_4]$ units in $\text{AgRE}^{\text{III}}\text{Si}_4$ and $[\text{NaQ}_6]$, $[\text{LaQ}_8]$, and $[\text{SiQ}_4]$ units in $\text{NaLaSi}_4^{\text{VI}}$. Due to the

fluctuations of the atomic radius and coordination numbers at the A-site, the compounds in the $A^I RE^{III} C^{IV} Q_4^{VI}$ family show a multiple structural transition from *Ama2* ($LiLaSiS_4$), *P2₁/c* ($Na/AgLaSiS_4$), and *P2₁* ($KLaSiS_4$) to *Pnma* ($Rb/CsLaSiS_4$). Moreover, the compounds exhibit wide band gaps (3.33 eV for $AgLaSiS_4$, 3.18 for $AgYSiS_4$, 3.83 eV (HSE06) for $NaLaSiS_4$, and 3.02 eV (HSE06) for $NaLaSiSe_4$) and large birefringence (0.114 for $AgLaSiS_4$, 0.129 for $AgYSiS_4$, 0.130 for $NaLaSiS_4$, and 0.160 for $NaLaSiSe_4$ at 1064 nm). It is worth noting that $NaLaSiSe_4$ exhibits the largest known birefringence in the $A^I RE^{III} C^{IV} Q_4^{VI}$ family compounds. DFT calculations unveil that the band gaps are enhanced by the charge transfer from $[REQ_8]$ to $[SiQ_4]$ in the title compounds and highlight that the layer distance affected birefringence in the isostructural compounds, which are beneficial for the regulation of the band gap and birefringence of advanced functional materials by similar chemical modulations.

Data availability statement

The authors declare that the main data that support the findings of this study are available within the article and the ESI.† Other relevant data are available from the authors upon reasonable request.

Conflicts of interest

The authors declare that they have no conflict of interest.

Acknowledgements

This work was supported by the Natural Science Foundation of Xinjiang Uygur Autonomous Region (2024D01E30), the National Natural Science Foundation of China (22335007, 52002398, 61835014, 51972336) and the Xinjiang Key Laboratory of Electronic Information Materials and Devices (2017D04029).

References

- 1 D. Mei, W. Cao, N. Wang, X. Jiang, J. Zhao, W. Wang, J. Dang, S. Zhang, Y. Wu, P. Rao and Z. Lin, Breaking through the “3.0 eV wall” of energy band gap in mid-infrared nonlinear optical rare earth chalcogenides by charge-transfer engineering, *Mater. Horiz.*, 2021, **8**, 2330–2334.
- 2 Y. Kang and Q. Wu, A review of the relationship between the structure and nonlinear optical properties of organic-inorganic hybrid materials, *Coord. Chem. Rev.*, 2024, **498**, 215458.
- 3 Y. Kang, C. Yang, J. Gou, Y. Zhu, Q. Zhu, W. Xu and Q. Wu, From $Cd(SCN)_2(CH_4N_2S)_2$ to $Cd(SCN)_2(C_4H_6N_2)_2$: controlling sulfur content in thiocyanate systems significantly improves the overall performance of UV nonlinear optical materials, *Angew. Chem., Int. Ed.*, 2024, **63**, e202402086.
- 4 M. Zhu, Y. Tang, X. Chen, L. Xu and X. Fan, B-N bonds between $SrBi_2B_2O_7$ and humic acid composites enhance polarized electric field for efficient piezocatalytic degradation of oxytetracycline in water, *Chem. Eng. J.*, 2024, **481**, 148379.
- 5 Y. Tang, X. Chen, M. Zhu, X. Liao, S. Hou, Y. Yu and X. Fan, The strong alternating built-in electric field sourced by ball milling on Pb_2BO_3X ($X = Cl, Br, I$) piezoelectric materials contributes to high catalytic activity, *Nano Energy*, 2022, **101**, 107545.
- 6 J. Li and F. L. Deepak, In situ kinetic observations on crystal nucleation and growth, *Chem. Rev.*, 2022, **122**, 16911–16982.
- 7 X. Wang, J. Li, Z. Zhao, S. Huang and W. Xie, Crystal structure and electronic structure of quaternary semiconductors $Cu_2ZnTiSe_4$ and Cu_2ZnTiS_4 for solar cell absorber, *J. Appl. Phys.*, 2012, **112**, 023701.
- 8 L. Wang, Q. Sun and J. Li, Recent progress on sulfide infrared nonlinear optical materials with large SHG response and wide band gap, *Chin. J. Struct. Chem.*, 2023, **42**, 100013.
- 9 G. Deokar, N. S. Rajput, J. Li, F. L. Deepak, W. Ou-Yang, N. Reckinger, C. Bittencourt, J. F. Colomer and M. Jouiad, Toward the use of CVD-grown MoS_2 nanosheets as field-emission source, *Beilstein J. Nanotechnol.*, 2018, **9**, 1686–1694.
- 10 Q. Wu, L. Kang and Z. Lin, A machine learning study on high thermal conductivity assisted to discover chalcogenides with balanced infrared nonlinear optical performance, *Adv. Mater.*, 2024, **36**, 2309675.
- 11 J. Xu, K. Wu, B. Zhang, H. Yu and H. Zhang, $LaAeAl_3S_7$ ($Ae = Ca, Sr$): cairo pentagonal layered thioaluminates achieving a good balance between a strong second harmonic generation response and a wide bandgap, *Inorg. Chem. Front.*, 2023, **10**, 2045–2052.
- 12 M. Yan, R. Tang, W. Xu, W. Liu and S. Guo, Centrosymmetric $CaBaMF_8$ and Noncentrosymmetric Li_2CaMF_8 ($M = Zr, Hf$): Dimension Variation and Nonlinear Optical Activity Resulting from an Isovalent Cation Substitution-Oriented Design, *Inorg. Chem.*, 2024, **63**, 5260–5268.
- 13 S. Liu, C. Li, J. Jiao, Y. She, T. Zhang, D. Ju, N. Ye, Z. Hu and Y. Wu, Three in one: a cadmium bismuth vanadate NLO crystal exhibiting a large second-harmonic generation response and enhanced birefringence, *Inorg. Chem. Front.*, 2024, **11**, 2384–2391.
- 14 W. Xie, R. Tang, S. Yan, N. Ma, C. Hu and J. Mao, $Ba_4B_{14}O_{25}$: a deep ultraviolet transparent nonlinear optical crystal with strong second harmonic generation response achieved by a boron-rich closed-loop strategy, *Small*, 2024, **20**, 2307072.
- 15 Z. Qian, H. Wu, Z. Hu, J. Wang, Y. Wu and H. Yu, $Cs_3In(In_4Se_7)(P_2Se_6)$: a multi-chromophore chalcogenide with excellent nonlinear optical property designed by group grafting, *Angew. Chem., Int. Ed.*, 2024, **63**, e202400892.

16 X. Li, Z. Shi, M. Yang, W. Liu and S. Guo, $\text{Sn}_7\text{Br}_{10}\text{S}_2$: the first ternary halogen-rich chalcohalide exhibiting a chiral structure and pronounced nonlinear optical properties, *Angew. Chem., Int. Ed.*, 2022, **61**, e202115871.

17 Q. Liu, X. Liu, L. Wu and L. Chen, SrZnGeS_4 : a dual-waveband nonlinear optical material with a transparency spanning UV/Vis and Far-IR spectral regions, *Angew. Chem., Int. Ed.*, 2022, **61**, e202205587.

18 X. Zhang, H. Wu, Z. Hu, J. Wang, Y. Wu and H. Yu, AlIIHgMIVS_4 (AlI = Sr, Ba, MIV = Si, Ge): a series of materials with large second harmonic generation response and wide band gaps, *Adv. Opt. Mater.*, 2024, **12**, 2301735.

19 X. Ji, H. Wu, B. Zhang, H. Yu, Z. Hu, J. Wang and Y. Wu, Intriguing dimensional transition inducing variable birefringence in $\text{K}_2\text{Na}_2\text{Sn}_3\text{S}_8$ and $\text{Rb}_3\text{NaSn}_3\text{Se}_8$, *Inorg. Chem.*, 2020, **60**, 1055–1061.

20 Z. Li, Y. Liu, S. Zhang, W. Xing, W. Yin, Z. Lin, J. Yao and Y. Wu, Functional chalcogenide $\text{Na}_2\text{HgSn}_2\text{Se}_6$ and $\text{K}_2\text{MnGe}_2\text{Se}_6$ exhibiting flexible chain structure and intriguing birefringence tunability, *Inorg. Chem.*, 2020, **59**, 7614–7621.

21 Z. Chen, W. Liu and S. Guo, A review of structures and physical properties of rare earth chalcophosphates, *Coord. Chem. Rev.*, 2023, **474**, 214870.

22 L. Dong, S. Zhang, P. Gong, L. Kang and Z. Lin, Evaluation and prospect of mid-infrared nonlinear optical materials in \mathcal{J} rare earth (RE = Sc, Y, La) chalcogenides, *Coord. Chem. Rev.*, 2024, **509**, 215805.

23 P. Feng, J. Zhang, M. Ran, X. Wu, H. Lin and Q. Zhu, Rare-earth-based chalcogenides and their derivatives: an encouraging IR nonlinear optical material candidate, *Chem. Sci.*, 2024, **15**, 5869–5896.

24 L. Gao, X. Wu, J. Xu, X. Tian, B. Zhang and K. Wu, Rational combination of multiple structural groups on regulating nonlinear optical property in hexagonal Ln_3MGeS_7 polar crystals, *J. Alloys Compd.*, 2022, **900**, 163535.

25 Y. Zhang, J. Chen, K. Li, H. Wu, Z. Hu, J. Wang, Y. Wu and H. Yu, $\text{LaMg}_6\text{Ga}_6\text{S}_{16}$: a chemical stable divalent lanthanide chalcogenide, *Nat. Commun.*, 2024, **15**, 2959.

26 H. Chen, Y. Zhang, Y. Yang and S. Guo, Ternary rare-earth sulfides RE_3GaS_6 (RE = Ho, Er): Crystal chemistry, second-order nonlinear optical properties and theoretical investigation, *J. Alloys Compd.*, 2021, **868**, 159112.

27 W. Yin, K. Feng, W. Wang, Y. Shi, W. Hao, J. Yao and Y. Wu, Syntheses, structures, optical and magnetic properties of $\text{Ba}_2\text{MLnSe}_5$ (M = Ga, In; Ln = Y, Nd, Sm, Gd, Dy, Er), *Inorg. Chem.*, 2012, **51**, 6860–6867.

28 Y. Yang, Y. Chu, B. Zhang, K. Wu and S. Pan, Unique unilateral-chelated mode-induced d–p– π interaction enhances second-harmonic generation response in new Ln_3LiMS_7 family, *Chem. Mater.*, 2021, **33**, 4225–4230.

29 A. Choudhury, L. A. Polyakova, I. Hartenbach, T. Schleid and P. K. Dorhout, Synthesis, structures, and properties of layered quaternary chalcogenides of the general formula ALnEQ_4 (A = K, Rb; Ln = Ce, Pr, Eu; E = Si, Ge; Q = S, Se), *Z. Anorg. Allg. Chem.*, 2006, **632**, 2395–2401.

30 P. Wu and J. A. Ibers, Synthesis and structures of the quaternary chalcogenides of the type KLnMQ_4 (Ln = La, Nd, Gd, Y; M = Si, Ge; Q = S, Se), *J. Solid State Chem.*, 1993, **107**, 347–355.

31 Y. Han, C. Hu, B. Li and J. Mao, LnLiSiS_4 (Ln = La and Ce): promising infrared nonlinear optical materials designed by aliovalent substitution from SrCdSiS_4 , *Mater. Today Phys.*, 2023, **31**, 100987.

32 G. Shi, Y. Wang, F. Zhang, B. Zhang, Z. Yang, X. Hou, S. Pan and K. R. Poeppelmeier, Finding the next deep-ultraviolet nonlinear optical material: $\text{NH}_4\text{B}_4\text{O}_6\text{F}$, *J. Am. Chem. Soc.*, 2017, **139**, 10645–10648.

33 X. Wang, Y. Wang, B. Zhang, F. Zhang, Z. Yang and S. Pan, $\text{CsB}_4\text{O}_6\text{F}$: a congruent-melting deep-ultraviolet nonlinear optical material by combining superior functional units, *Angew. Chem., Int. Ed.*, 2017, **56**, 14119–14123.

34 Z. Zhang, Y. Wang, B. Zhang, Z. Yang and S. Pan, Polar fluorooxoborate, $\text{NaB}_4\text{O}_6\text{F}$: a promising material for ionic conduction and nonlinear optics, *Angew. Chem., Int. Ed.*, 2018, **57**, 6577–6581.

35 A. Abudurusuli, J. Huang, P. Wang, Z. Yang, S. Pan and J. Li, $\text{Li}_4\text{MgGe}_2\text{S}_7$: the first alkali and alkaline-earth diamond-like infrared nonlinear optical material with exceptional large band gap, *Angew. Chem., Int. Ed.*, 2021, **60**, 24131–24136.

36 X. Chen, Q. Jing and K. M. Ok, $\text{Pb}_{18}\text{O}_8\text{Cl}_{15}\text{I}_5$: a polar lead mixed oxyhalide with unprecedented architecture and excellent infrared nonlinear optical properties, *Angew. Chem., Int. Ed.*, 2020, **59**, 20323–20327.

37 Y. Chu, H. Wang, Q. Chen, X. Su, Z. Chen, Z. Yang, J. Li and S. Pan, “Three-in-One”: a new Hg-based selenide $\text{Hg}_7\text{P}_2\text{Se}_{12}$ exhibiting wide infrared transparency range and strong nonlinear optical effect, *Adv. Funct. Mater.*, 2024, **34**, 2314933.

38 O. V. Dolomanov, L. J. Bourhis, R. J. Gildea, J. A. K. Howard and H. Puschmann, OLEX2: a complete structure solution, refinement and analysis program, *J. Appl. Crystallogr.*, 2009, **42**, 339–341.

39 M. Mutailipu, J. Han, Z. Li, F. Li, J. Li, F. Zhang, X. Long, Z. Yang and S. Pan, Achieving the full-wavelength phase-matching for efficient nonlinear optical frequency conversion in $\text{C}(\text{NH}_2)_3\text{BF}_4$, *Nat. Photonics*, 2023, **17**, 694–701.

40 B. Zhang, G. Shi, Z. Yang, F. Zhang and S. Pan, Fluorooxoborates: beryllium-free deep-ultraviolet nonlinear optical materials without layered growth, *Angew. Chem., Int. Ed.*, 2017, **56**, 3916–3919.

41 M. Mutailipu, M. Zhang, B. Zhang, L. Wang, Z. Yang, X. Zhou and S. Pan, $\text{SrB}_5\text{O}_7\text{F}_3$: the first asymmetric alkaline-earth fluorooxoborate with unprecedented $[\text{B}_5\text{O}_9\text{F}_3]^{6-}$ functionalized chromophore, *Angew. Chem., Int. Ed.*, 2018, **57**, 6095–6099.

42 X. Lou, X. Jiang, B. Liu and G. Guo, Excellent nonlinear optical $\text{M}[\text{M}_4\text{Cl}][\text{Ga}_{11}\text{S}_{20}]$ (M = A/Ba, A = K, Rb) achieved by unusual cationic substitution strategy, *Small*, 2024, **20**, 2305711.

43 H. Wang, X. Pan, W. Zhao, Y. Chu and J. Li, A new infrared nonlinear optical material BaZnGeS_4 with wide band gap

and large nonlinear optical response, *Inorg. Chem. Front.*, 2023, **10**, 6253–6261.

44 L. Wang, D. Chu, Z. Yang, J. Li and S. Pan, Wide band gap selenide infrared nonlinear optical materials $\text{AlIMg}_6\text{Ga}_6\text{Se}_{16}$ with strong SHG responses and high laser-induced damage thresholds, *Chem. Sci.*, 2024, **15**, 6577–6582.

45 N. Pienack and W. Bensch, The new silver thiostannate (1, 4–dabH₂) Ag_2SnS_4 : solvothermal synthesis, crystal structure and spectroscopic properties, *Z. Anorg. Allg. Chem.*, 2006, **632**, 1733–1736.

46 Y. Wu and W. Bensch, Syntheses, crystal structures and spectroscopic properties of $\text{Ag}_2\text{Nb}[\text{P}_2\text{S}_6][\text{S}_2]$ and $\text{KAg}_2[\text{PS}_4]$, *J. Solid State Chem.*, 2009, **182**, 471–478.

47 A. Grzegorczyk, J. Z. Zheng, D. Wright and P. F. McMillan, LaSe_{2-x} compounds: Vibrational and electrical properties, *J. Phys. Chem. Solids*, 1996, **57**, 1625–1634.

48 H. Wang, Y. Chu, X. Pan, Z. Yang, S. Pan and J. Li, Double alkaline earth metals sulfide SrMgGeS_4 with high laser-induced damage threshold and strong second-harmonic generation, *Mater. Today Phys.*, 2023, **38**, 101243.

49 J. Zhou, Z. Fan, K. Zhang, Z. Yang, S. Pan and J. Li, $\text{Rb}_2\text{CdSi}_4\text{S}_{10}$: novel $[\text{Si}_4\text{S}_{10}]$ T2-supertetrahedra-contained infrared nonlinear optical material with large band gap, *Mater. Horiz.*, 2023, **10**, 619–624.

50 A. P. Litvinchuk, V. M. Dzhagan, V. O. Yukhymchuk, M. Y. Valakh, I. S. Babichuk, O. V. Parasyuk, L. V. Piskach, O. D. Gordian and D. R. Zahn, Electronic structure, optical properties, and lattice dynamics of orthorhombic $\text{Cu}_2\text{CdGeS}_4$ and $\text{Cu}_2\text{CdSi}_4\text{S}_4$ semiconductors, *Phys. Rev. B: Condens. Matter Mater. Phys.*, 2014, **90**, 165201.

51 I. Hartenbach and T. Schleid, Thiosilicate der selten-erd-elemente: III. $\text{KLa}[\text{Si}_4\text{S}_4]$ und $\text{RbLa}[\text{Si}_4\text{S}_4]$ – ein struktureller vergleich, *Z. Anorg. Allg. Chem.*, 2005, **631**, 1365–1370.

52 M. Usman, M. D. Smith, G. Morrison, V. V. Klepov, W. Zhang, P. S. Halasyamani and H.-C. zur Loye, Molten alkali halide flux growth of an extensive family of noncentrosymmetric rare earth sulfides: structure and magnetic and optical (SHG) properties, *Inorg. Chem.*, 2019, **58**, 8541–8550.

53 Y. Chu, H. Wang, T. Abutukadi, Z. Li, M. Mutailipu, X. Su, Z. Yang, J. Li and S. Pan, $\text{Zn}_2\text{HgP}_2\text{S}_8$: a wide bandgap Hg-based Infrared nonlinear optical material with large second-harmonic generation response, *Small*, 2023, **19**, 2305074.

54 M. Zhang, B. Liu, X. Jiang and G. Guo, Nonlinear optical sulfides $\text{LiMg}_{1-x}\text{Ga}_x\text{S}_{14}$ ($\text{M} = \text{Rb/Ba, Cs/Ba}$) created by Li^+ driven 2D centrosymmetric to 3D noncentrosymmetric transformation, *Small*, 2023, **19**, 2302088.

55 Y. Han, C. Hu and J. Mao, $\text{Ca}_2\text{Ln}(\text{BS}_3)(\text{Si}_4\text{S}_4)$ ($\text{Ln} = \text{La, Ce, and Gd}$): mixed metal thioborate–thiosilicates as well-performed infrared nonlinear optical materials, *Small*, 2023, **19**, 2302088.

56 K. Ding, H. Wu, Z. Hu, J. Wang, Y. Wu and H. Yu, $[\text{Ba}_4(\text{S}_2)][\text{ZnGa}_4\text{S}_{10}]$: design of an unprecedented infrared nonlinear salt-inclusion chalcogenide with disulfide-bonds, *Small*, 2023, **19**, 2302819.

57 R. Li, Q. Liu, X. Liu, Y. Liu, X. Jiang, Z. Lin, F. Jia, L. Xiong, L. Chen and L. Wu, $\text{Na}_2\text{Ba}[\text{Na}_2\text{Sn}_2\text{S}_7]$: structural tolerance factor-guided NLO performance improvement, *Angew. Chem., Int. Ed.*, 2023, **62**, e202218048.

58 M. Ran, S. Zhou, W. Wei, B. Li, X. Wu, H. Lin and Q. Zhu, Rational design of a rare-earth oxychalcogenide $\text{Nd}_3[\text{Ga}_3\text{O}_3\text{S}_3][\text{Ge}_2\text{O}_7]$ with superior infrared nonlinear optical performance, *Small*, 2023, **19**, 2300248.

59 A. O. Okorogu, S. B. Mirov, W. Lee, D. I. Crouthamel, N. Jenkins, A. Y. Dergachev, K. L. Vodopyanov and V. V. Badikov, Tunable middle infrared downconversion in GaSe and AgGaS_2 , *Opt. Commun.*, 1998, **155**, 307–312.

60 W. Zhou, W. Yao, Q. Zhang, H. Xue and S. Guo, Introduction of Li into Ag-based noncentrosymmetric sulfides for high-performance infrared nonlinear optical materials, *Inorg. Chem.*, 2021, **60**, 5198–5205.

61 W. Zhou, M. Geng, M. Yan, N. Suen, W. Liu and S. Guo, Alkali metal partial substitution-induced improved second-harmonic generation and enhanced laser-induced damage threshold for Ag-based sulfides, *Inorg. Chem. Front.*, 2022, **9**, 3779–3787.

62 W. Xing, N. Wang, C. Tang, C. Li, Z. Lin, J. Yao, W. Yin and B. Kang, From AgGaS_2 to AgHgPS_4 : vacancy defects and highly distorted HgS_4 tetrahedra double-induced remarkable second-harmonic generation response, *J. Mater. Chem. C*, 2021, **9**, 1062–1068.

63 J. Xu, Y. Xiao, K. Wu, B. Zhang, D. Lu, H. Yu and H. Zhang, Flexible anionic groups-activated structure dissymmetry for strong nonlinearity in $\text{Ln}_2\text{Ae}_3\text{MIV}_3\text{S}_{12}$ family, *Small*, 2024, **20**, 2306577.

64 Y. Shi, Y. Chen, M. Chen, L. Wu, H. Lin, L. Zhou and L. Chen, Strongest second harmonic generation in the polar R_3MTQ_7 family: atomic distribution induced nonlinear optical cooperation, *Chem. Mater.*, 2015, **27**, 1876–1884.

65 W. Xing, C. Tang, N. Wang, C. Li, Z. Li, J. Wu, Z. Lin, J. Yao, W. Yin and B. Kang, EuHgGeSe_4 and EuHgSnS_4 : two quaternary Eu-based infrared nonlinear optical materials with strong second-harmonic-generation responses, *Inorg. Chem.*, 2020, **59**, 18452–18460.

66 W. Xing, N. Wang, Y. Guo, Z. Li, J. Tang, K. Kang, W. Yin, Z. Lin, J. Yao and B. Kang, Two rare-earth-based quaternary chalcogenides EuCdGeQ_4 ($\text{Q} = \text{S, Se}$) with strong second-harmonic generation, *Dalton Trans.*, 2019, **48**, 17620–17625.

67 P. Wang, Y. Chu, A. Tudi, C. Xie, Z. Yang, S. Pan and J. Li, The combination of structure prediction and experiment for the exploration of alkali-earth metal-contained chalco-pyrite-like IR nonlinear optical material, *Adv. Sci.*, 2022, **9**, e2106120.

68 L. Luo, L. Wang, J. Chen, J. Zhou, Z. Yang, S. Pan and J. Li, $\text{AlBII}_3\text{CIII}_3\text{QVI}_8$: a new family for the design of infrared nonlinear optical materials by coupling octahedra and tetrahedra units, *J. Am. Chem. Soc.*, 2022, **144**, 21916–21925.

69 Y. Liu, X. Li, S. Wu, M. Ma, X. Jiang, Y. Wu and D. Mei, A rare earth chalcogenide nonlinear optical crystal KLaGeS₄: achieving good balance among band gap, second harmonic generation effect, and birefringence, *Inorg. Chem.*, 2024, **63**, 10938–10942.

70 L. Wang, C. Tu, H. Gao, J. Zhou, H. Wang, Z. Yang, S. Pan and J. Li, Clamping effect driven design and fabrication of new infrared birefringent materials with large optical anisotropy, *Sci. China: Chem.*, 2023, **66**, 1086–1093.